Journal of Orthopaedic Translation 49 (2024) 167–180

Contents lists available at ScienceDirect

Journal of Orthopaedic Translation

journal homepage: www.journals.elsevier.com/journal-of-orthopaedic-translation

Original Article

A biodegradable magnesium phosphate cement incorporating chitosan and rhBMP-2 designed for bone defect repair

Peng He [a,1], Yanbin Zhao [b,c,1], Bin Wang [a,1], Guoyin Liu [a], Lei Zhang [a], Mei Li [d], Bin Xu [a], Weihua Cai [e,**], Chenglin Chu [b,c,***], Yu Cong [a,*]

[a] Department of Orthopedics, Jinling Hospital, Affiliated Hospital of Medical School, Nanjing University, Nanjing, 211166, China
[b] School of Materials Science and Engineering, Southeast University, Nanjing, 211189, China
[c] Jiangsu Key Laboratory for Advanced Metallic Materials, Southeast University, Nanjing, 211189, China
[d] Medical Research Center, Department of Orthopedics, Guangdong Provincial People's Hospital, Guangdong Academy of Medical Sciences, Guangzhou, 510080, China
[e] Department of Orthopedics, The First Affiliated Hospital of Nanjing Medical University, Nanjing, 210029, China

A B S T R A C T

Background: The repair of bone defects has always been a significant challenge in clinical medicine. To address this challenge, doctors often utilize autologous bone grafts, allogeneic bone grafts and artificial bone substitutes. However, the former two methods may result in additional trauma and complications, while allogeneic bone grafts carry the risks of immune rejection and disease transmission. Magnesium phosphate cement (MPC), as a artificial bone substitutes, has been a potential biomaterial for repairing bone defects, but its clinical application is limited by insufficient mechanical strength and poor osteoinductive activity.

Methods: In this study, the cement liquid phase base on rhBMP-2 and chitosan solution into MPC were obtained and investigated. After mixing with a cement liquid, the structural and phase composition, morphology, chemical structure, setting time, compressive strength, degradation behavior, solubility, and cellular responses and bone regeneration in response to CHI-rhBMP2 MPC were investigated in vitro and in vivo.

Results: After the chemical component modification, CHI-rhBMP2 MPC possessed controllable degradation rate, moderate setting time, appropriate cuing temperature, good injectability, and improved initial strength. In vitro tests showed that the CHIrhBMP2 MPC could promote cell proliferation and adhesion, as well as that contribute to osteoblast differentiation and mineralization. In addition, cement materials were implanted into the rabbit femoral condyles for in vivo osseointegration evaluation. The results displayed that more new bone grew around CHI-rhBMP2 MPC, verifying improved osseointegration capacity. Transcriptome analysis revealed that focal adhesion, Forkhead box O (FoxO) signaling pathway and P13K/AKT signaling pathway were may involved in CHI-rhBMP2 MPC induced new bone formation.

Conclusion: This work provides a new strategy for the rational design of potential bone repair candidate materials.

1. Introduction

In clinical, trauma, infection, osteoporosis, and bone tumor often cause large bone defects. How to fill bone defects has always been a thorny problem for orthopedic surgeons. At present, autologous bone and allogeneic bone are commonly used as bone defect fillers in clinical practice [1]. However, there are some problems such as sampling difficulty, infection and rejection in implant site, pain in bone harvesting area [2–4]. Thus, how to find suitable replacement bone repair materials has become the most concerned problem for researchers.

Artificial bone repair materials, particularly inorganic bone cement, have attracted extensive attention from researchers due to their excellent biocompatibility, bioactivity, injectability, mouldability and unrestricted Source. PMMA bone cement is the commonly used as bone repair materials, and has the advantages of excellent shape, curing, used in osteoporosis fracture and bone defect, but the existence of high curing temperature, toxic, difficult to degradation, bone growth hard faults was hindered their further clinical applications [5,6]. Calcium phosphate cement(CPC)as 1980s began to study a new type of bone cement filling material. CPC bone grafts have been widely researched for bone repair due to the good self-setting ability, injectability, mouldability, biocompatibility, osteoconductivity, resorbability, and feasibility in controlled drug delivery [7–10]. Unfortunately, the critical limitations of CPC include poor mechanical strength, high brittleness, poor anti-washout

* Corresponding author. Department of Orthopedics, Jinling Hospital, Affiliated Hospital of Medical School, Nanjing University, Nanjing, 211166, China.
** Corresponding author.
*** Corresponding author.
E-mail addresses: caiwhspine@sina.com (W. Cai), clchu@seu.edu.cn (C. Chu), congyu122@126.com (Y. Cong).
[1] These authors contributed equally to this work.

https://doi.org/10.1016/j.jot.2024.08.004
Received 3 February 2024; Received in revised form 4 August 2024; Accepted 5 August 2024

behaviour, and lack of osteogenic property have hampered its application [7,11].

Magnesium phosphate cement (MPC), as an emerging alternative biomaterial, was first reported and applied to the medical materials in 1990s. MPC was gradually entered the field of view of scientific researchers because of the controllable degradation rate, appropriate solidification time and higher initial strength, which overcame the disadvantages of CPC. Apart from above merits, MPCs also exhibit excellent biocompatibility and relatively closer to the mechanical properties of cortical bone representing further promising properties for a potential clinical use [12–14].Traditional MPC is consisted of the hydration of ammonium dihydrogen phosphate ($NH_4H_2PO_4$) and dead burn magnesia (MgO). It was found that the emission of ammonia gas during the hydration process may be cytotoxic and adverse to bone regeneration and wound healing. Subsequently, researchers successfully explored that replacing $NH_4H_2PO_4$ with potassium dihydrogen phosphate (KH_2PO_4) could avoid ammonia release. Meanwhile, potassium MPC has short setting time for injection and vulnerable to washout until hardening occurs, and it generates significant heat during setting [15].

Modifications to potassium MPC composition would be making for improving its properties such as adding bioactive substances [15–18]. Chitosan, as a nontoxic, biocompatible, and biodegradable natural polysaccharide, has been proverbially known as an additive for orthopedic bioengineering applications and drug delivery system. Gong et al. [15] indicated that incorporated O-CMC, an O-carboxymethyl derivative of Chitosan, to MPC (OMPC) could increase the compressive strength and setting time of K-struvite and decrease its porosity and pH value. Furthermore, OMPC remarkably improved the proliferation, adhesion, and osteogenesis related differentiation of MC3T3-E1 cells. Liu et al. [18] reported that incorporating Tricalcium silicate (C3S) into MPC could enhance the mechanical strength to 87 MPa, that was close to the human vertebral cortical bone. Subsequent biological experiments revealed that C3S/MPC showed good cytocompatibility and stimulatory effect on the proliferation of MC3T3-E1 osteoblast cells than MPC *in vitro*. Shi et al. [19] demonstrated that incorporated Chondroitin sulfate (CS) into MPC to improve its properties. The results showed that the setting time was extended from 6 min to 16 min with an increase in CS content from 0 % to 5 %. 2.5 % CS-MPC had the highest compressive strength of 30 MPa, which was 58 % higher than that of MPC. Furthermore, CS-MPC had a more neutral pH than MPC. These CS-modified cements promoted pre-osteoblast cell proliferation, attachment, and differentiation *in vitro* and enhanced bone formation *in vivo*. Therefore, the incorporation of bioactive substances is a valid method to control its hydration and degradation rate and enhance the biological properties of bone cement at the same time.

In the case of a good bone regeneration capacity of the patient, a complete degradation of the implant within about six months would be desirable [20]. In recent years, it became apparent that the degradation rate of magnesium phosphate is likely to be closer to the ideal of a rapid, complete replacement of the implant by new bone tissue, while exhibiting a similarly good biocompatibility [21,22]. But the lack of excellent osteoinductivity and osteogenic still significantly impact the osseointegration of bone cements and eventually result the failure of bone repair, especially the reconstruction of large bone defect. Bone morphogenetic protein-2 (BMP-2), as a member of transforming growth factor-β (TGF-β) superfamily, is a promising growth factor for bone regeneration. Proper amounts of BMP-2 not only accelerate osteogenesis at bone defect sites, improve the success rate of bone non-union healing, but also promote the generation of blood vessels at bone repair sites [23,24]. A major challenge in biomedical applications is finding an optimal carrier for its delivery at the site of injury and bone defects. Inorganic calcium phosphate-based scaffolds have already been investigated as carriers of BMP-2 individually [25,26]. Thus, we speculated that magnesium phosphate bone cement could also be used as the ideal carrier of rhBMP-2 to the site of bone defect and there have been no reports to date of the addition of rhBMP-2 into magnesium phosphate bone cements.

Herein, we attempt to incorporate rhBMP-2 and chitosan into MPC in order to obtain controllable degradation rate, appropriate solidification time and higher initial strength while maintaining excellent cytocompatibility and osteoinductivity. In this study, characterizations of physicochemical and degradation behaviour were performed in detail. whereafter, cellular responses and bone regeneration in response to these MPC samples were investigated *in vitro* and *in vivo*. Finally, the potential molecular mechanisms that promoted osteogenic differentiation were investigated by Transcriptome sequencing (Fig. 1).

2. Materials and methods

2.1. Fabrication of cements

The light magnesium oxide (l-MgO) and potassium dihydrogen phosphate (KH_2PO_4) were all in A.R. grade and both purchased from Sinopharm Chemical Reagent Co., Ltd. The light MgO was calcined at 1600 °C for 4 h to obtain the dead-burnt magnesium oxide (d-MgO). After grinding, KH_2PO_4 and d-MgO were sieved and their average particle sizes were about 75 and 50 μm, respectively. The MPCs powers were prepared by uniformly mixing KH_2PO_4 and d-MgO at a mass ratio of 1: 1.5. Chitosan (CHI, 100 kDa) and phosphoric acid were obtained from Shanghai Aladdin Biochemical Technology Co., Ltd, as well as Recombinant Human Bone Morphogenetic Protein 2 (rhBMP2, Bone Repairing Material) was acquired from Hangzhou Jiuyuan Gene Engineering Co., Ltd. Then, the powers were admixed with MPCs liquid phase (ultrapure water, CHI solution, or CHI-rhBMP2 blend) to form the H_2O MPCs, CHI MPCs and CHI-rhBMP2 MPCs. Herein, CHI solution was fabricated by dissolving 2.5 mg/mL of chitosan into 1 wt% of acetic acid, and then the pH was set to 4.0 with phosphoric acid. After that, the CHI solution was mixed with 0.01 mg/mL of rhBMP2 to prepared the CHI-rhBMP2 blend. After preliminary experiments, the power to liquid ratios (PLRs) of H_2O MPCs, CHI MPCs and CHI-rhBMP2 MPCs were 5: 1, 5: 1.125, and 5: 1.125, separately. The H_2O MPCs were used as the control groups in this study.

The MPCs power and liquid phase were homogeneously mixed by a fine glass rod for 30 s to form a paste, which was then transferred to a cylindrical silicone mold (9 mm in diameter and 5 mm in height for *in vitro* assays, or 3 mm in diameter and 10 mm in height for *in vivo* experiment). After solidification, cement samples were washed with water and cured in an incubator (37 °C, 100 % humidity) for 24 h to prevent hydration reaction.

2.2. Characterization of cements

The morphology and elements of MPCs were measured by Field-emission scanning electron microscopy (FE-SEM, Nova Nano SEM 450, FEI, USA) equipped with an energy-dispersive X-ray spectrometer (EDS). The phase compositions of samples were tested by an X-ray diffraction (XRD, Bruker D8-Discover, Germany), with a Cu target at a scanning rate of 0.15°/s, and the diffraction patterns were gathered from 10° to 65°. The chemical composition of the materials was analyzed using Fourier transform infrared spectroscopy (FT-IR, Thermo Scientific Nicolet iS10, USA). The acid-base properties of cements were evaluated by immersing specimens into the phosphate-buffered saline (PBS, initial pH = 7.4) in tubes for 24 h with a pH meter. The mass (g) to volume (mL) ratio was 0.2: 1.

2.3. Setting time and exothermic analysis

The setting time of MPCs were characterized by a standard Vicat apparatus. The prepared paste-like cements were quickly moved to a silicone mold ($\varphi 10 \times 10$ mm^3). The period from mixing powder with liquid phase until the needle of the Vicat instrument cannot penetrate the cements for more than 1 mm is recorded as the setting time. At least three parallels were performed to ensure the reliability of the data. At

the same time, the temperature changes of MPCs in fabrication procedure were also monitored with an infrared thermogram (UNI-T, UTi120s, China).

2.4. Injectability and anti-washout property of MPCs

The injectability of cements were measured according to Refs. [27, 28].In the process of cements fabrication, the solid and liquid components of cements were mixed by hand for 1 min, after which the resulting paste was transferred into a 10 mL syringe with an inner diameter of 14.5 mm. A 16 G metal cannula with an outer diameter of 1.65 mm, an inner diameter of 1.19 mm, and a wall thickness of 0.22 mm was attached to the syringe. The syringes with cannulas were then securely fixed in a vertical position on a custom stand, positioned between the knock plates of a compression machine. The cement paste was injected into the cannula at a constant rate of 15 mm/min, with the load being recorded as a function of the plunger displacement. The test was concluded once the applied load reached a force of 120 N. The injectability percentage was calculated using the following Equation (1).

$$Injectability\ ratio\ (\%) = \frac{W_F - W_A}{W_F - W_E} \times 100\% \quad (1)$$

where the weight of the empty syringe is denoted as WE, the weight of the syringe filled with paste is denoted as WF, and the weight of the syringe after injection with any remaining paste is denoted as WA.

To assess wash-out resistance, different cement paste mixtures were prepared and filled into syringes, which were then manually injected into Ringer's solution at 37 °C. A sample was deemed to demonstrate wash-out resistance if no apparent disintegration was observed in the solution within a 30-min period.

2.5. Compressive strength and porosity

The compressive strength of cement was tested using a universal testing machine (XQY-II, China) with a 1 mm/min of loading rate. At least five duplicate pairs were carried out for each group. The porosity of sample was evaluated after curing for 24 h by an electronic densimeter (AR-300G, China) according to Archimedes' principle. In brief, as-prepared MPCs were soaked in ultrapure water until saturated and the porosity (%) was calculated by Eq. (2):

$$Porosity(\%) = \frac{W_2 - W_1}{W_2 - W_3} \times 100\% \quad (2)$$

where W_1 and W_2 represented the weights of specimens before and after infiltration, as well as the suspended mass of soaked MPCs was denoted W_3.

2.6. In vitro degradation behavior

The degradation behavior of cements *in vitro* was carried out by immersing specimens into PBS (pH 7.4) for 28 days. Briefly, in initial masses of MPCs solidified at 37 °C in 100 % humidity for 24 h were weighted and recorded as M_0. Then, they were soaked in PBS at 37 °C with a solid-to-liquid ratio of 20: 1 (mL/g). After certain time, cements were taken out and dried in a draught drying cabinet at 40 °C for 12 h, and their masses were denoted M_1, as well as the pHs of solutions were recorded. The weight loss rate (WLR, %) of MPCs was calculated according to Eq. (3):

$$WLR(\%) = \frac{M_0 - M_1}{M_0} \times 100\% \quad (3)$$

The morphology of the immersed cements was observed using SEM, as well as EDS was applied to detect the elements of surface.

2.7. Hemolysis assay

The Hemolysis test was approved by the Ethics Committee at Jinling Hospital, China. The MPC samples were placed in a 24-well plate with 1.5 mL saline solution for 30 min at 37 °C. Then, 30 μL diluted blood (fresh human blood/saline solution = 4/5) was added and the mixture was incubated for 60 min. Furthermore, 30 μL diluted blood was added to saline and distilled water as the negative and positive controls, respectively. Then, the mixtures were collected, centrifuged at 3000 rpm for 5 min, and the absorbance of the supernatant was detected at 545 nm. The hemolysis rate (HR) was calculated using the following equation:

$$\text{Hemolysis} = (A_{sample} - A_{negative})/(A_{positive} - A_{negative}) \quad (4)$$

where, A_{sample}, $A_{negative}$, and $A_{positive}$ are the absorbance values of the sample, and negative and positive controls, respectively.

2.8. Cell culture

MPC samples were immersed in culture medium with a ratio of 200 mg/mL as previous study described [29]. After incubated at 37 °C for 24 h, the culture extracts was collected and stored at 4 °C for further use. C3H10T1/2 cells (donated by the Medical Research Center of Guangdong Provincial People's Hospital) were cultured at 37 °C with 5 % CO_2 in low glucose DMEM (Gibco; Thermo Fisher Scientific, Inc.) supplemented with 10 % FBS (Gibco; Thermo Fisher Scientific, Inc.) and 0.1 % streptomycin/penicillin. The culture medium was changed every 2 days and the cells were passaged at ~85 % confluence.

2.9. Cytocompatibility assays

C3H10T1/2 Cells (1×10^4 cells/well) were cultured in extracts of the cement samples for 1, 3, and 5 days. Cell proliferation and cytotoxicity was analyzed by CCK-8 assay (DOJINDO, Japan). The absorbance of the culture medium was measured at 450 nm wave length using a microplate reader. Cell viability was detected by Live/Dead staining after 3d of culture. Briefly, the samples were washed three times with PBS, and live and dead cells on the samples were stained with calcein-AM (2 μM) and propidium iodide (PI, 5 μM) for 15 min at 37 °C. Finally, cell viability was observed using a fluorescence microscope.

Cells were directly cultured on different MPC samples for 3 days. Then cells were fixed with 4 % paraformaldehyde for 15 min and washed three times with PBS.F-actin was stained with acti-stain 555 phalloidin (Servicebio, Wuhan, China) for 1 h, while nuclei were counterstained by 4′,6-diamidino-2-phenylindole (DAPI). Afterwards, the fluorescence images were observed and captured using fluorescence microscopy (FV1200; Olympus, Tokyo, Japan).

2.10. Alkaline phosphate (ALP) activity assay

Each MPC sample was immersed in 1 mL α-minimum essential medium (α-MEM) for 24 h to prepare the extracts, which were supplemented with 10 mM β-glycerophosphate, 100 nM dexamethasone, 50 mM ascorbate and glutamine for osteogenic induction. Cells (1×10^4 cells/well) were seeded in 24-well plates for 24 h and then the culture medium was replaced with various extracts. The intracellular ALP was stained on days 7 and 14 using 5-bromo-4-chloro-3-indolyl-phosphate (BCIP)/nitro blue tetrazolium (NBT) ALP color development kit (Beyotime, China) for ALP staining. Furthermore, ALP activities were quantitatively evaluated by ALP detection assay kit (Beyotime Biotechnology, China).

2.11. Extracellular matrix (ECM) mineralization assay

The degree of extracellular matrix (ECM) mineralization in

C3H10T1/2 cells cultured as described in section 2.10 above was evaluated on day 7 and 14 using Alizarin Red (Cyagen, China). Briefly, cells were rinsed with PBS, fixed with 75 % ethanol, stained with 40 mM Alizarin Red and then rinsed with deionized water to eliminate nonspecific staining. The staining results were imaged using a inverted phase contrast microscope (Olympus, Germany). For the quantitative analysis, 10 % cetylpyridinium chloride (Sigma Aldrich USA) was used to dissolve the mineralized nodules and then the absorbance of the resultant reaction solution was measured at 560 nm.

2.12. Quantitative real-time PCR assays

Expression of osteogenesis-related genes was evaluated by quantitative real-time polymerase chain reaction(qRT-PCR). Briefly, total RNA was extracted using the TRIzol method and cDNA was synthesized with the RevertAid first-strand cDNA synthesis kit (Thermo Fisher Scientific, Waltham, MA, USA) according to the manufacturer's instructions. Realtime PCR amplification was detected using the ABI PRISM 7900HT fast sequence detection system (Thermo Fisher Scientific). The expression of osteogenesis-related genes, including alkaline phosphatase (ALP), runt-related transcription factor (Runx2), osteocalcin (OCN), and collagen type 1 (COL1), was normalized to β–actin using the $2^{-\Delta\Delta Ct}$ method. The primer sequences are listed in Table 1.

2.13. In vivo animal experiments

The *in vivo* experiments were reviewed and approved by the Investigational Ethical Review Board of Jinling Hospital of Nanjing Medical University (approval number:2022DZGKJDWLSS-0024). Twenty-four New Zealand white rabbits were randomly divided into four groups with preset sampling time of 6 and 12 weeks for the current study. The operations were performed in an operating room under aseptic conditions. Under general anesthesia (3 % pentobarbital) and sterile conditions, the femur of each rabbit was randomly exposed and A hole (4 mm in diameter) was drilled in the distal condyles part of the femur. Cylindrical preset samples of MPC (4 mm in diameter and 10 mm in length) were implanted into the defects in the rabbit femora and periosteum was layered sutured. The blank control group (Sham) was not implanted with any materials. All animals were sacrificed by an overdose of pentobarbitone after implantation for 6 and 12 weeks.

2.14. Micro-CT scan and histological analysis

After implantation for 6 and 12 weeks, the rabbits were sacrificed and the distal condyles part of the femur obtained for analysis. The femurs were evaluated using micro-computed tomography (micro-CT; Aloka Latheta LCT-200, HITACHI, Japan) and then the three-dimensional (3D) images were reconstructed using Scanco Medical software. For cylindrical implant areas, the following data were analyzed by the software: BV/TV, BMD, TP. th, and TP. Sp.

For the histological examinations, the fixed femurs were dehydrated in a series of graded concentrations of ethanol, embedded in polymethyl methacrylate (PMMA), cut into 200 μm sections, and then ground into 50 μm pieces. Subsequently, the femurs with implants were collected and fixed in 4 % paraformaldehyde. After gradient dehydration and embedding in polymethylmethacrylate, tissues were cut into sections by using a saw microtome (EXAKT Apparatebau, Germany). Then, VG staining was performed on the sections polished to about 50 μm, and the representative pictures were acquired using a microscope (Olympus, Japan). The osseous tissues were decalcified in EDTA decalcifying solution for 4 weeks, and then, the implants were removed gently from the femurs. The decalcified femurs were then dehydrated, embedded, and then cut into 5 μm-thick slices. Afterward, the obtained sections were dewaxed in xylene and hydrated in gradient ethanol. Through antigen retrieval and blocking, the sections were incubated with primary antibodies (COL-I, OCN; Servicebio, China) and the goat anti-rabbit IgG secondary antibody (InvivoGen, USA). Finally, the positive protein expression was detected by 3,3′-diaminobenzidine solution (Dako, Denmark) and the hematoxylin counterstaining process and examined using a microscope.

Table 1
Primer sequences used for real-time PCR amplification.

Gene name	Forward sequence	Reverse sequence
GAPDH (human)	CAAGAGCACAAGAGGAAGAGG	CTACATGGCAACTGTGAGGAG
GAPDH (mouse)	TTCCAGGAGCGAGACCCCACTA	GGGCGGAGATGATGACCCTTTT
Runx2	GACTGTGGTTACCGTCATGGC	ACTTGGTTTTTCATAACAGCGGA
ALP	TCCGTGGGCATTGTGACTAC	TGGTGGCATCTCGTTATCCG
OCN	GGTAGTGAACAGACTCCGGC	GGCGGTCTTCAAGCCATACT
COL1	GCTCCTCTTAGGGGCCACT	ATTGGGGACCCTTAGGCCAT

2.15. RNA sequencing and differentially expressed gene analysis

C3H10T1/2 cells cultured in the extract of H_2O MPC and CHI-rhBMP2 samples were collected, and the total RNA was extracted by Trizol reagent (Invitrogen). RNA purity was determined and quantified using a Nano Drop 2000 spectrophotometer. Transcriptome sequencing and analysis were performed by JIKAI Biotech Co. Clean reads were obtained by comparing reference genes using Trimmomatic software, hisat2. Fragments per kilobase of exon per million reads mapped were quantified using cufflinks software. Volcano plot and heatmap were used to show the differential genes with P values less than 0.05 and difference fold greater than 2. Gene Ontology (GO), Kyoto Encyclopedia of Genes and Genomes (KEGG) and Gene Set Enrichment Analysis (GSEA) enrichment analysis of differential transcripts were performed.

2.16. Statistics

Statistical analyses were performed using SPSS v21.0 (IBM Statistics, Chicago, IL). All data are reported as means ± standard deviations. For comparisons, one way ANOVA was used to determine significant differences between groups. Differences with $P < 0.05$ were considered statistically significant (see Fig. 1).

3. Results and discussion

3.1. Characterization of MPC samples

The SEM morphologies of cements were showed in Fig. 2a–c. The H_2O MPC mainly consisted of phosphate crystals with many cracks. In contrast, with the incorporations of chitosan or CHI-rhBMP2 liquid phases, these fissures were filled with polymer and the surface become dense and smooth. In Fig. 2d, XRD was used to detect the phase composition of cements and displayed typical peaks of $KMgPO_4{\cdot}6H_2O$ and the remained MgO. The results indicated that the addition of chitosan or CHI-rhBMP2 has no significant effect on the physical phase of MPC after cementation. Fig. 2e showed the chemical groups found in the cements. In the case of MPC, peaks at 565 and 1642 cm^{-1} were identified as PO_4^{3-} groups. CHI MPC displayed C=O (1708 cm^{-1}) and -OH (3419 cm^{-1}) groups, indicating the presence of CHI in the cements. Additionally, vibrational modes at 1365 and 1445 cm^{-1} corresponded to C-N bonds and N-H stretching in CHI, respectively. The sulfuric acid bond was detected at 1120 cm^{-1} due to the incorporation of rhBMP2. These findings confirm the successful inclusion of CHI and AMP rhBMP2 in the CHI-rhBMP2 sample.

Bone cement needs to have sufficient compressive strength for clinical applications [30,31]. In Fig. 2f, the compressive strength of control group was 66.95 MPa, yet the CHI and CHI-rhBMP2 MPCs increased, ~1.1- and ~1.3-fold stronger than it. The compressive strength of

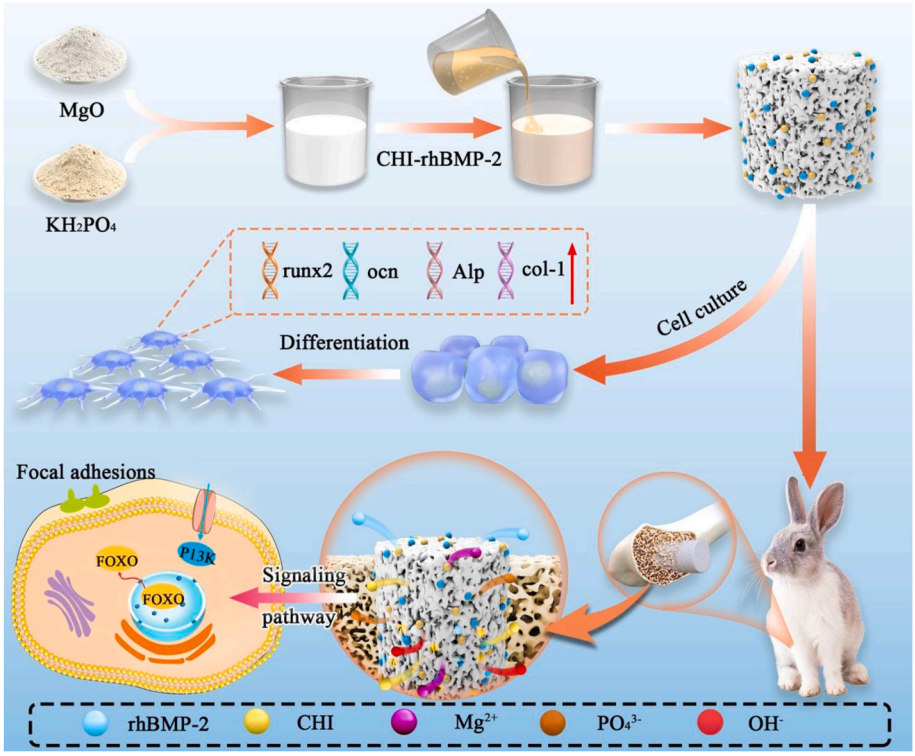

Fig. 1. Schematic illustration of the CHI-rhBMP2 MPC sample preparation and its enhanced biocompatibility and osteogenesis activity *in vitro* and *in vivo*.

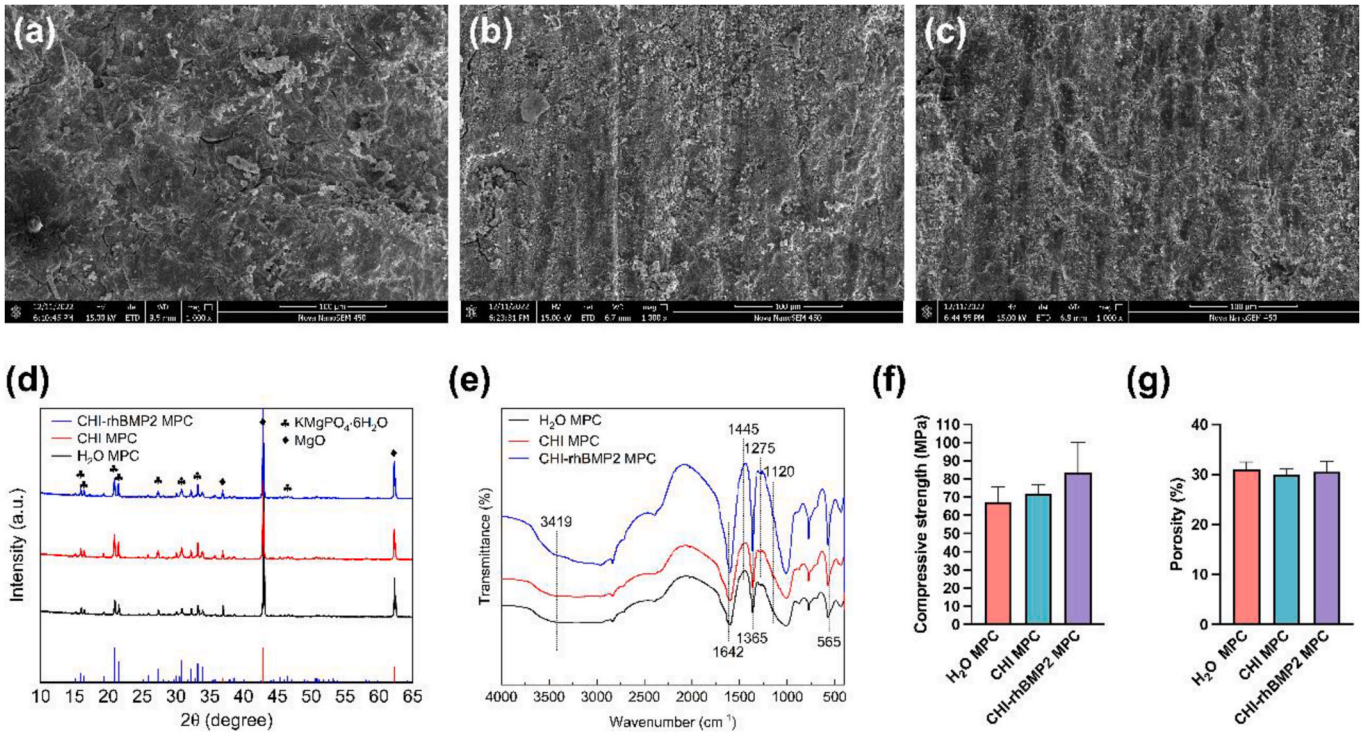

Fig. 2. Morphologies of (a) H_2O MPC, (b) CHI MPC, and (c) CHI-rhBMP2 MPC. (d) XRD of MPCs. (e) FT-IR of MPCs. (f) Compressive strengths of MPCs. (g) Porosity of MPCs.

CHI-rhBMP2 MPCs was higher than that of clinical polymethyl methacrylate (PMMA, 24–50 MPa) and calcium phosphate cements (20–40 MPa). It demonstrated that the incorporation of chitosan and rhBMP2 enhanced the compressive strength of cements. Besides, the porous structure of materials was conducive to promote angiogenesis and bone formation [32]. The porosities of MPC samples were around 30 % in Fig. 2g, which could provide a suitable space for the growth of osteoblasts and vessels.

3.2. Physical and chemical properties of MPC samples

Cellular activity is closely related to the surrounding microenvironment that includes pH value and temperature [19,33]. The hydration reaction between KH_2PO_4 and d-MgO leads to the high alkalinity of bone cement, and thus it is necessary to acidify the liquid phase of bone cement to neutralize the alkalinity. In Fig. 3a, the pH of CHI and CHI-rhBMP2 solutions were 4.21 and 4.03, which showed stronger acidity compared with ultrapure water (pH 7.39). After curing (Fig. 3b), H_2O MPC as the control exhibited strong alkalinity (pH 10.19), but both the pH of CHI and CHI-rhBMP2 MPCs were around 7.35–7.50, which similar in human body PH value(7.35–7.45), indicating a suitable

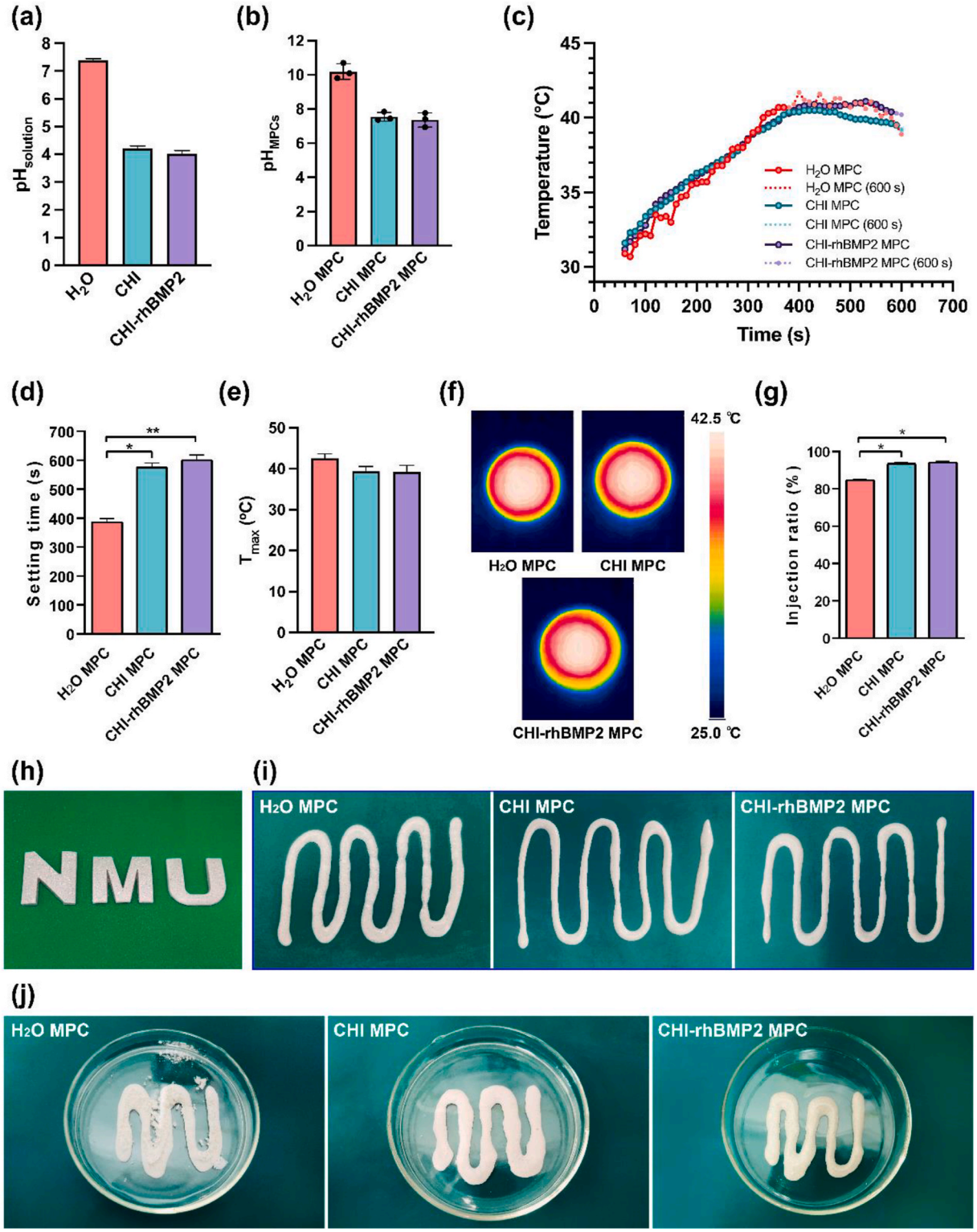

Fig. 3. (a) pH of cements liquid phase. (b) pH of MPC. (c) Temperature changes during MPCs fabrication. (d) Setting time of cements. (e) The maximum temperature in hydration reaction. (f) Infrared thermal radiation images of MPCs. (g) Injection rate of MPCs. (h) School logo of Nanjing Medical University made by cements. (i) Representative images of the injectability of cements. (j) Representative images of anti-washout property of cements. (*p < 0.05; **p < 0.01; ***p < 0.001).

environment for cells growth. Temperature variation during the fabrication of MPCs was performed in Fig. 3c. The heat changes showed a trend of increasing first and then decreasing steadily.

The setting time of bone cement is a key consideration in clinical applications. The ideal setting time ranging from 8 to 15 minis appropriate for clinal practical use [34]. In Fig. 3d, the setting time increased with the incorporation of chitosan and rhBMP2. The hydration reaction of cements was very quick, which caused the setting time to be only about 6 min. By contrary, the setting time of CHI MPCs was deferred to 9.6 min, which was due to the addition of chitosan. For CHI-rhBMP2 MPC, whose liquid phase was the mixture of chitosan and rhBMP2, the setting time increased to 10 min. The maximum temperature (T_{max}) of H_2O MPC was 42.5 °C, while decreased when adding chitosan and rhBMP2 as shown in Fig. 3e. And the infrared thermal radiation images of the corresponding MPCs were showed in Fig. 3f. Therefore, the incorporation of chitosan and rhBMP2 prolonged the setting time and reduced the exothermic reaction of cements.

Injectability can be defined as the ability of a paste to extrude through the syringe [35]. This is another important indicator for measuring the practicality of bone cements. In Fig. 3g, only 84.5 % of

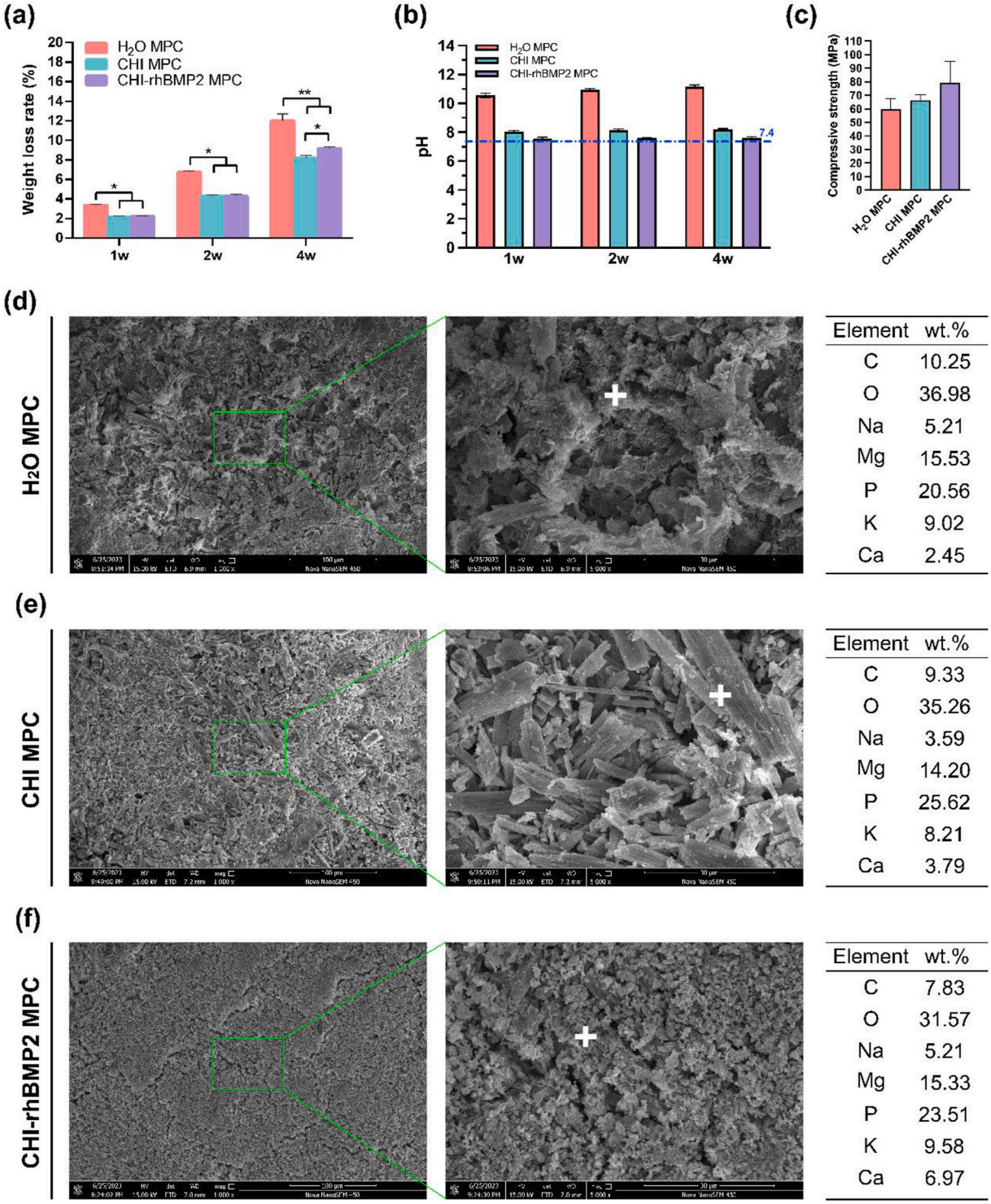

Fig. 4. (a) Weight loss rate, (b) pH, (c) Compressive strength, (d-f)SEM images and EDS results of MPCs after 28 d of immersion in PBS. (*p < 0.05; **p < 0.01).

H_2O cement could be extruded from 2.5 mL syringes. However, the injection rates of both CHI and CHI-rhBMP2 MPCs increased to 93.3 % and 94.0 %, respectively. Fig. 3h showed the school logo made by CHI-rhBMP2 MPC. The representative images of injectable cements were also observed in Fig. 3i. It could be seen that the injection rates of CHI-rhBMP2 MPC was improved compared with H_2O MPC and CHI MPC. Furthermore, the CHI MPC and CHI-rhBMP2 MPC exhibited better anti-washout property than H_2O MPC due to the addition of CHI and rhBMP2 as shown in Fig. 3j.

3.3. Degradation behavior of MPC samples

The biomaterials should have the gradually degrade after providing support for bone repair, and the degradation rate should match the growth rate of new bone [36]. In Fig. 4a, the incorporation of chitosan and rhBMP2 has an inhibitory effect on the degradation rate of bare cements. Especially in 28 d, the WLR of H_2O MPC was 11.98 %, but decreased to 8.23 % and 9.17 %, respectively. At the same time, in Fig. 4b, it could be seen that both CHI and CHI-rhBMP2 MPCs maintained the comfortable pH (~7.35–7.4) within 28 d of immersion in PBS, suggesting that CHI and CHI-rhBMP2 still has potential advantages at 28d after implantation. The compressive strengths of cements after degradation were also measured in Fig. 4c. The CHI-rhBMP2 MPC stilled kept the best mechanical strength with a strength of 79.46 MPa. In Fig. 4d–f, scanning electron microscopy (SEM) images clearly illustrate that the surface of H_20 MPC exhibits noticeably porous features following degradation, with CHI-MPC following suit. In contrast, CHI-rhBMP2 maintained a relatively dense surface. These findings provide further evidence that H_20-MPC degrades at the fastest rate and CHI-rhBMP2 displays superior corrosion resistance. Additionally, energy-dispersive spectroscopy (EDS) results suggest that degradation products primarily consist of CaP, which is beneficial for promoting biocompatibility. Notably, CHI-rhBMP2 MPC was found to have the highest calcium content, which is likely to be advantageous for enhancing bone healing processes (see Fig. 5).

3.4. The biological compatibility of MPC samples

Biocompatibility of MPC samples was tested by using hemolysis test, a standard CCK-8 assay, and live/dead staining. The HR of each sample was measured because it is a critical parameter and is expected to be <5 % for clinical applicability [37,38]. Fig. 4a showed the HR values of the chitosan and rh-BMP-2 modified samples were <5 %, which met the requirement. In Fig. 4b, after incubating with C3H10T1/2 cells for 1 day, there was no difference upon the viable cells among the three MPC samples. The viability of cells on the samples increased with culture time,the proliferation capability of the CHI-rhBMP2 MPC sample was much higher than those of the H_2O MPC sample and CHI MPC sample for 3 and 5 days. Furthermore, cells cultured for 4 days were analyzed using the live/dead staining test. In Fig. 4c, more live cells (green) were observed on the CHI MPC and CHI-rhBMP2 MPC samples than H_2O MPC sample, which was consistent with the proliferation results. Taken together, these results proved that incorporating chitosan and rhBMP-2 in MPC could considerably improve the biocompatibility without any cytotoxicity *in vitro*.

Cell adhesion occurs in the early stage of tissue regeneration, and effective cell adhesion provides the basis for subsequent biological functions, including cell proliferation and differentiation [39,40].Cell morphology and adhesion were directly assessed using fluorescence imaging as shown in Fig. 4d. After 24 h of culture on the samples, cells adhered to the surfaces,fiber-like structures were seen on all MPC samples and the pseudopodia between cells fused with each other, indicating favorable biocompatibility for all MPC cement groups. It was interesting to find that, with the incorporating chitosan, cells formed more pseudopodia and were distributed more widely, especially when the rhBMP-2 was added. Previous studies have indicated this phenomenon that magnesium-chitosan was found to have conducive characteristics to protein adsorption and can provide a good platform for cell adhesion and proliferation [41].

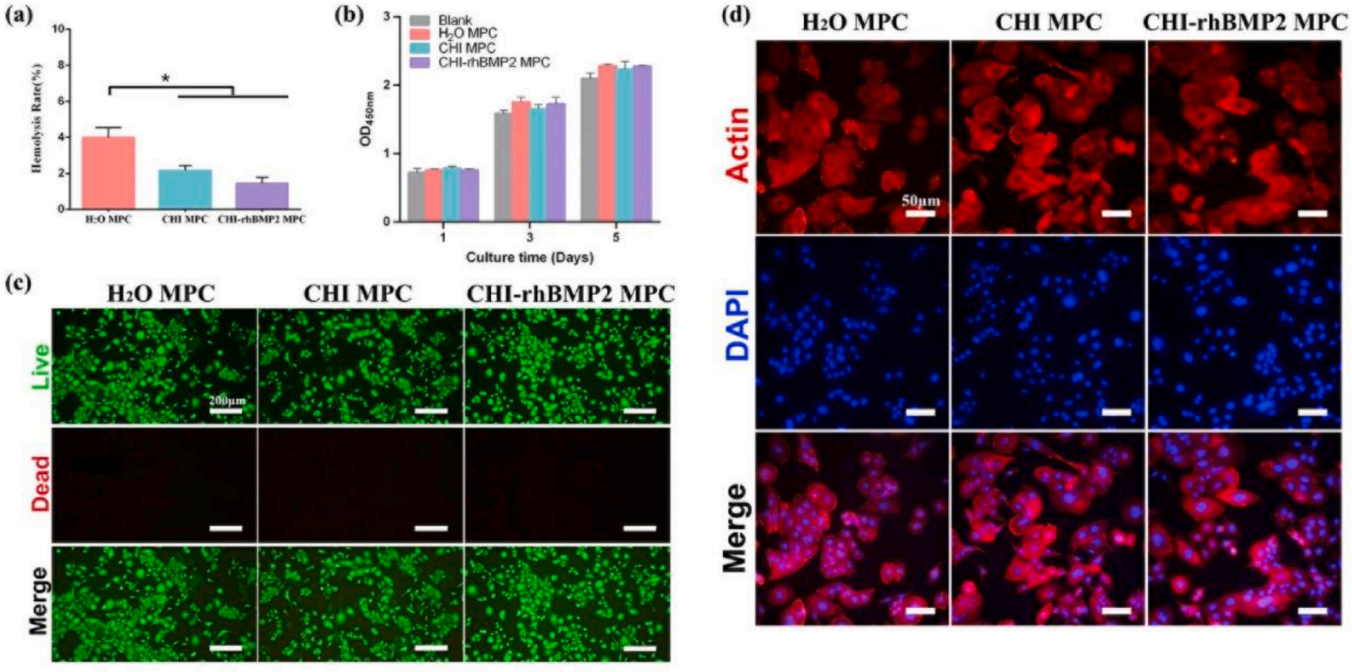

Fig. 5. In vitro evaluation of biocompatibility: (a) Hemolysis rate, (b) Cell proliferation and cytotoxicity evaluated by CCK-8 (c). Fluoroscopy images of live/dead (green/red) staining of C3H10T1/2 cells cultured in the extract of the different MPC samples for 3 days (scale bar = 200 μm). and (d) Immunofluorescent images of F-actin marker, red) expression in C3H10T1/2 cells cultured on different MPC samples (scale bar = 50 μm). (*p < 0.05; **p < 0.01; ***p < 0.001). (For interpretation of the references to colour in this figure legend, the reader is referred to the Web version of this article.)

3.5. Osteogenic differentiation behaviors of samples in vitro

The functional role of osteoblasts in bone formation is divided into three main stages: the first stage is the adhesion and proliferation of osteoblasts; the second stage is osteogenic differentiation, which is the process of differentiation and maturation of osteoblasts from osteogenic precursor cells into osteoblasts; the third stage is extracellular matrix mineralization, in which mature osteoblasts form a bone matrix through calcium and phosphorus eposition [42,43].Our experiments have demonstrated that CHI-rhBMP2 MPC group can promote the adhesion and proliferation of C3H10T1/2 osteogenic precursor cells. Alkaline phosphatase enzymatic activity reflects osteoblast function and is a surrogate of osteogenic differentiation [44].Subsquently, the ALP activities of C3H10T1/2 cells were quantitively and qualitatively evaluated for the early osteogenic differentiation. As shown in Fig. 7a, ALP could hydrolyze the 5-Bromo-4-chloro-3-indolyl phosphate (BCIP) and form an insoluble, dark blue or purple blue formazan CHI-rhBMP2 MPC group displayed denser and deeper ALP positive staining after 7 and 14 days. In addition, CHI-rhBMP2 MPC group is favorable for elevating the ALP activity(Fig. 7b)at day 7 and day 14 compared to the other two groups ($p < 0.05$).At the same time,the mineral precursors most include calcium and phosphate rich materials and the deposition of calcium matrix can be stained with Alizarin Red Staining (ARS). In Fig. 6d, there was no significant difference in the three groups at day 7, but the corresponding qualitative and quantitative results of matrix mineralization results at 14 day (Fig. 6c and d) suggested that the mineralization level

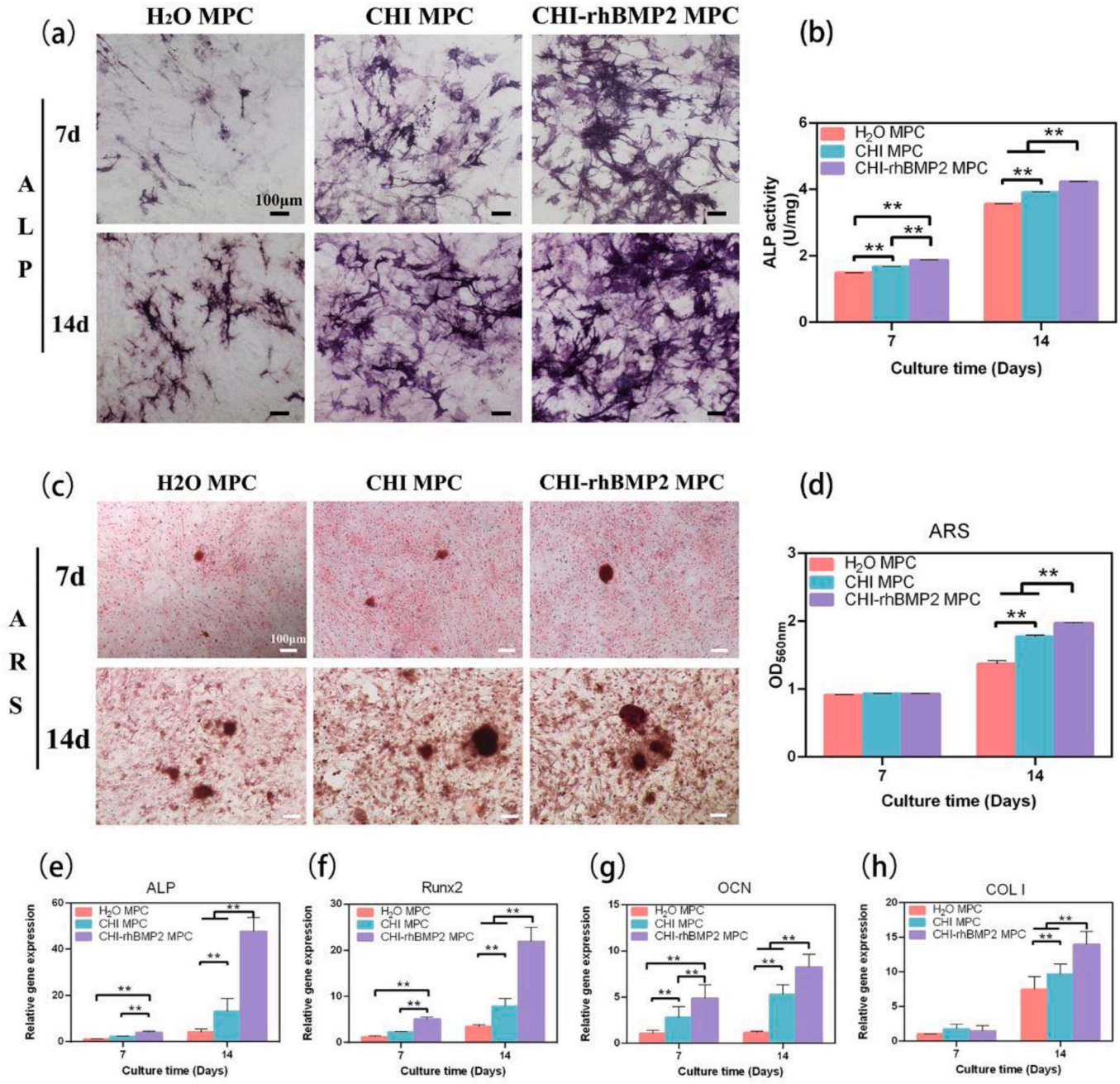

Fig. 6. In vitro evaluation of osteogenesis. (a) ALP staining of C3H10T1/2 treated with different MPC samples for 7 and 14 days (scale bar = 100 μm); (b) Quantitative analysis of ALP activity; (c) ARS staining and (d) quantitative results of ECM mineralization of C3H10T1/2 cultured on different MPC samples for 7 and 14 days (scale bar = 100 μm). (e–h) The expression of osteogenesis-related genes of C3H10T1/2 cells cultured on different MPC samples for 7 and 14 days. (*: $p < 0.05$, **: $p < 0.01$ and ***: $p < 0.001$).

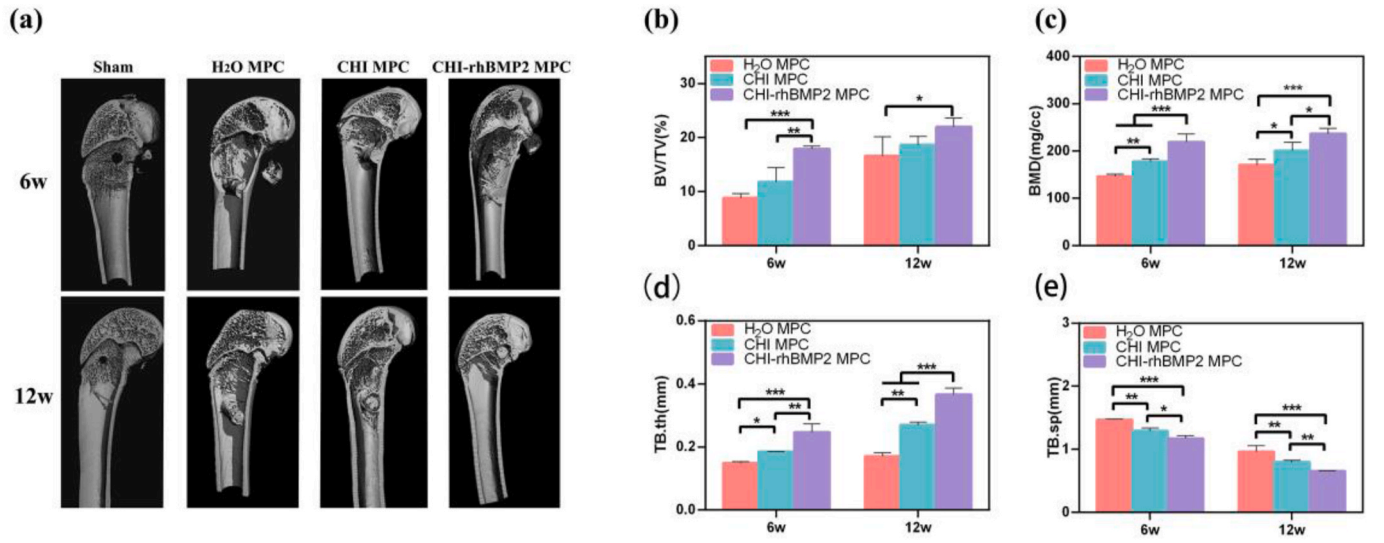

Fig. 7. Radiological assessment of the osteogenic effect *in vivo*. (a) Three-dimensional reconstruction images of Micro-CT results of the different MPC samples after implantation in femur of rabbits for 6 and 12 weeks. (b–e) Quantitative analysis of the osteogenic effect from BV/TV, BMD, TB.Th, and TB.Sp after implantation in femur of rabbits for 6 and 12 weeks. (*: $p < 0.05$, **: $p < 0.01$ and ***: $p < 0.001$).

of ECM in the CHI-rhBMP2 MPC group was higher than in the other groups($p < 0.001$), and these all results indicated that the early ALP activity and the amount of mineralized nodules formation in the CHI-rhBMP2 MPC group were greater elevated than that of H_2O MPC and CHI MPC groups.

The osteoblasts produce many cell products, including ALP, growth factors, hormones such as OCN, and collagen, part of the organic unmineralized component of the bone called osteoid. As we all known, COL1 is an important component of the bone matrix produced by osteoblasts, OCN is a more abundant non-collagenous protein in the bone matrix and ALP is typical protein product produced by osteoblasts, both of which are important for osteoblast adhesion, differentiation and bone matrix formation [44–46]. Runx2 is a transcription factor, which binds to core-binding factor subunit-β to form a heterodimer, that regulates the expression of osteoblast genes such as those encoding osteopontin (*Spp1*), bone sialoprotein 2 (*Ibsp*) and osteocalcin 2 (*Bglap2*) [47,48]. In this study, the osteogenesis-related genes of C3H10T1/2 cells was examined at the transcriptional level. As shown in Fig. 7, the expression of the Alp, Runx2 and Ocn genes was significantly higher in the CHI-rhBMP2 MPC group and CHI MPC group than in the H_2O MPC group both at day 7 and day 14 ($P < 0.05$),Meanwhile, the expression of the Alp, Runx2 and Ocn genes in the CHI-rhBMP2 MPC group were higer 1–3 fold than CHI MPC group and the difference between two groups was significant ($P < 0.05$). In terms of Col1 genes, as shown in Fig. 6f, there was no significant difference in the three groups at day 7, but the expression of the Col1 genes was higher in the CHI-rhBMP2 MPC group than in the CHI MPC and H_2O MPC groups at 14 day($P < 0.01$). Genetic studies demonstrated that BMP-2 could upregulate the expression of the osteogenic lineage genes, osterix (Osx) and Ocn significantly, and also induce Runx2 expression [24,47,49]. Our experiments are consistent with these results that add rhBMP-2 into CHI MPC could upregulate the expression of Alp, Runx2,Ocn and Col1 genes, suggesting that CHI-rhBMP2 MPC promote osteogenic differentiation and has the excellent osteoinductivity *in vitro*.

3.6. Osteogennic differentiation behaviors of samples in vivo

To further examine the osteointegration capacity *in vivo*, a bone-implant model was used. The same size of bone defect was drilled and three MPC groups were implanted into it to observe the degradation behavior and new bone formation. After 6 and 12 weeks, the implanted pillars were scanned using micro-CT and the 3D-reconstructed images with and without the newly formed bone around the implants are showed in Fig. 7a. Micro-CT images suggested that the cortical bone defect was still clearly visible in the sham group at 6 weeks and 12 weeks, and the bone defect at 12 weeks was somewhat smaller than the defect at 6 weeks, but it was still clearly visible, so the defect had not been completely repaired. Compared with three implant groups,we could see that CHI-rhBMP2 MPC implant had the largest most consolidated bony callus compared to the other groups at both weeks 6 and 12, which was further validated by the quantitative BV/TV values shown in Fig. 7b. In parallel, the quantitative analysis results shown in Fig. 7c demonstrated that the BMD of the bone surrounding the CHI-rhBMP2 MPC implants was larger than that surrounding the CHI MPC and H_2O MPC implants at 6 and 12 weeks after operation ($P < 0.05$). In Fig. 7d,at 6 week and 12 week, the trabecular thickness(Tb.th)of bone in the CHI-rhBMP2 MPC group were significantly thicker than that H_2O MPC and CHI MPC groups and there was significant difference among the three groups, respectively($P < 0.05$). By contrast, CHI-rhBMP2 MPC group in Fig. 7e could significantly reduce the trabecular separation(Tb.sp)of bone than H_2O MPC and CHI MPC groups. Thus, the changes of aforementioned parameters of the micro-CT analysis indicate that CHI-rhBMP2 MPC can induce in the greatest bone growth at 6 weeks, with higher bone regeneration even at later time points at 12 weeks among three MPC materials.

On the other hand, the osteointegration ability of the implants was also evaluated histologically. The bone around implants was stained red through Van Gieson's (VG) staining for undecalcified sections. As shown in Fig. 8a, there were only a few new bone tissues surrounding the H_2O MPC implant group. By contrast, completed new bone circles were formed in CHI MPC and CHI-rhBMP2 MPC pillars. Interesting, new bone circles in CHI-rhBMP2 MPC group was thicker than CHI MPC group. Simultaneously, the special markers (Ocn, Col1) of osseointegration were immunohistochemically stained on decalcified histological sections. Our results shown in Fig. 9b and c indicated that CHI-rhBMP2 MPC and CHI MPC groups exhibited most OCN and Col1 expression around the implants during bone reconstitution a 12 weeks after surgery. Notably, larger stained areas and deeper positive staining were observed around the CHI-rhBMP2 MPC group than CHI MPC groups. Therefore, our results confirmed that the incorporating rhBMP-2 into CHI MPC implants effectively promoted the osseointegration *in vivo*.

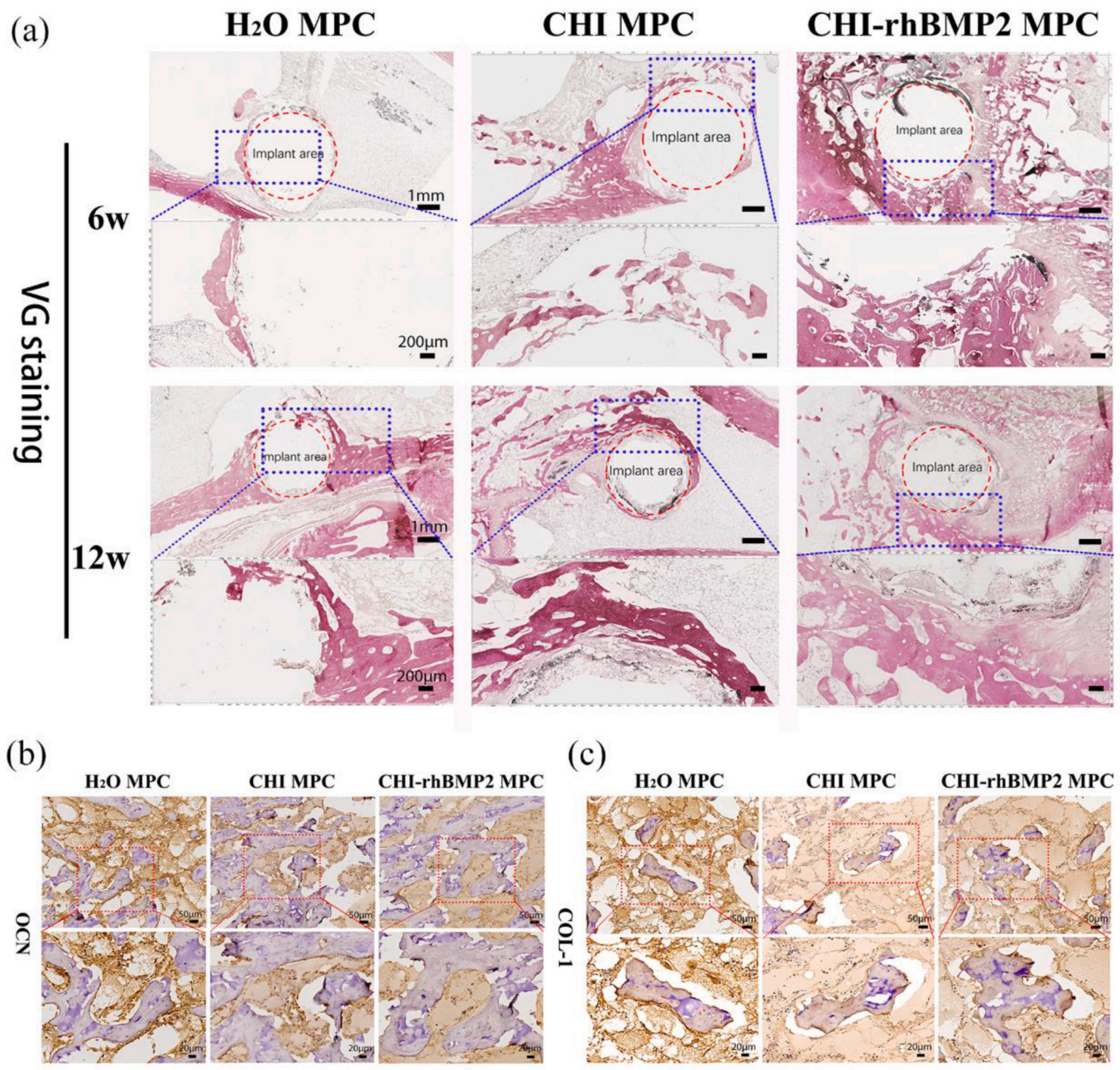

Fig. 8. Histological assessment of the osteogenic effect *in vivo*(a)VG staining of different MPC samples after femur implantation for 6 and 12 weeks. (b) OCN staining and (c) COL1 staining of the different samples after femur implantation for 12 weeks.

3.7. Transcriptome sequencing to analyze the potential mechanisms of osteogenesis

RNA-Seq are critical to deciphering the structure and function of the genome and identifying changes in relevant signaling pathways [50]. C3H10T1/2 cells cultured on H_2O MPC and CHI-rhBMP2 samples for 3 days for RNA sequencing. There were totally 5119 specific genes by the RNA-Seq, and CHI-rhBMP2 MPC group upregulated 2683 genes and downregulated 2436 genes compared with H_2O MPC group (Fig. 9a). Cluster analysis heatmap screened out the genes of CHI-rhBMP2 that showed differences compared with the H_2O MPC (P values < 0.05) (Fig. 9b). These different expression genes may play essential roles in the field of osteogenesis, to explore the specific function, we use GO enrichment analysis to figure out the key functions from three main part: molecular function, cellular component and biological process firstly, the results showed that different expression genes may accelerate the process of osteogenesis by regulation of cytoskeleton organization, regulation of protein complex assembly, intrinsic apoptotic signaling pathway and regulation of mitotic cell cycle (Fig. 9c and d). Moreover, we investigate the potential pathways by KEGG and GSEA methods. Our results shown in Fig. 9e-f demonstrated that CHI-rhBMP2 MPC positively regulated C3H10T1/2 cells proliferation and osteogenic differentiation may via Focal adhesion, FoxO signaling pathway and P13K/AKT signaling pathway. Among the various pathways, Focal adhesion, FoxO signaling and PI3K AKT signaling pathway have been evidenced that promote cells ossification [51–54]. In conclusion, the differential expression and bioinformatic analysis have given a positive inclination that CHI-rhBMP2 MPC could release the chitosan and rhBMP2 which induced the C3H10T1/2 cells osteogenesis effectively by key molecular functions and pathways mentioned before. Although

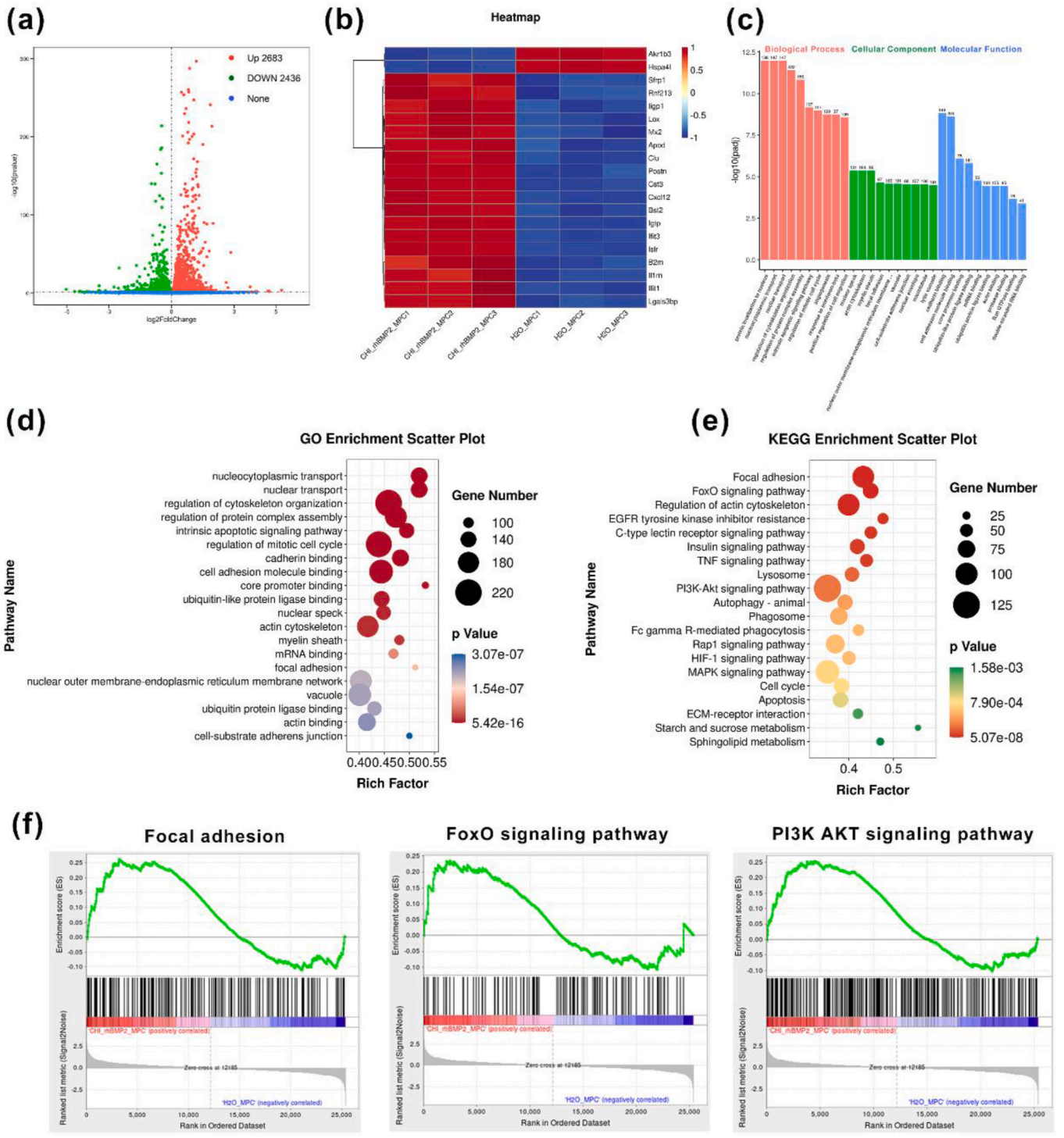

Figure 9. Transcriptome sequencing analysis of the mechanism of CHI-rhBMP2 MPC regulating bone formation. (a) Volcano plot of RNA-seq results. (b) The different expression genes between CHI-rhBMP2 and H_2O MPC. (c) (d) GO enrichment analysis of DEGs. (e) KEGG enrichment analysis of DEGs. (e) GSEA analysis of Focal adhesion, FoxO and P13K/AKT signaling pathways.

these finds need further confirmation by *in vivo* and vitro experiments, these showed CHI-rhBMP2 MPC plays a crucial role in the osteogenic differentiation process and provides evidence for subsequent mechanism exploration and research.

4. Conclusions

The ideal goal for a bone graft is to be osteoconductive, osteoinductive, and osteogenic, while minimizing risks to the patient. In our research, we successfully attempted to incorporate rhBMP-2 and chitosan into MPC and thereby obtaining controllable degradation rate, moderate setting time, appropriate reaction temperature and higher initial strength while maintaining excellent cytocompatibility. Furthermore, this study evaluated the effects of CHI-rhBMP2 MPC on C3H10T1/2 cells proliferation and osteogenic differentiation *in vitro*, as well as the potential underlying mechanism. The results demonstrated that CHI-rhBMP2 MPC positively regulated C3H10T1/2 cells proliferation and osteogenic differentiation may via Focal adhesion, FoxO signaling

pathway and P13K/AKT signaling pathway inducing new bone formation. Meanwhile, CHI-rhBMP2 MPC showed better and faster osteogenesis and osteoinductivity, with enhanced formation and thickening of new bone tissue than the other in rabbit model. To that end, the use of injectable MPC incorporating chitosan and rhBMP-2 validates a novel and translational therapeutic approach for improving bone repair. From animal experimentation to the eventual application of any bone substitute material in humans, this process involves lengthy and intricate stages. Our research is currently in its infancy, and further validation of the CHI-rhBMP2 MPC material's performance is imperative, encompassing its osteogenic mechanism, degradation mechanism, metabolic pathway, and ultimately, its ability to achieve complete degradation. This may involve subsequent verification steps utilizing large animal models. Ultimately, we aspire for this material to be applied clinically sooner and faster, bringing respite to patients with bone defects.

The translational potential of this article

This study presents a novel magnesium phosphate cement (MPC) formulation incorporating chitosan and rhBMP-2, which demonstrates enhanced osseointegration and bone regeneration capabilities. The developed material exhibits controllable degradation, improved mechanical properties, and favorable cellular responses, making it a promising candidate for bone defect repair. The findings of this research have significant clinical implications, offering a potential alternative to traditional bone grafting methods with reduced risks and complications. The successful in vivo evaluation in rabbit models further supports its translational potential for future clinical applications.

Funding statement

This research did not receive any specific grant from funding agencies in the public, commercial, or not-for-profit sectors.

Declaration of competing interest

The authors declare that they have no known competing financial interests or personal relationships that could have appeared to influence the work reported in this paper.

Acknowledgments

This research was financially supported by National Natural Science Foundation of China (No. 52171236, 51971062, 82102547), Open Research Fund of Jiangsu Key Laboratory for Advanced Metallic Materials, Southeast University (No. AMM2021A01) and General Fund of Scientific Research Project of Jiangsu Provincial Health Commission (No. H2019022).

References

[1] Baldwin P, Li DJ, Auston DA, Mir HS, Yoon RS, Koval KJ, et al. Bone graft substitutes: clinical evidence and indications for use in the setting of orthopaedic trauma surgery. J Orthop Trauma 2019;33(4):203–13.
[2] Valtanen RS, Yang YP, Gurtner GC, Maloney WJ, Lowenberg DW. Synthetic and Bone tissue engineering graft substitutes:what is the future? Injury 2021;52:S72–7.
[3] Campana V, Milano G, Pagano E, Barba M, Cicione C, Salonna G, et al. Bone substitutes in orthopaedic surgery: from basic science to clinical practice. J Mater Sci Mater Med 2014;25(10):2445–61.
[4] Betz RR. Limitations of autograft and allograft: new synthetic solutions. Orthopedics 2002;25(5 Suppl):s561–70.
[5] Gillman CE, Jayasuriya AC. FDA-approved bone grafts and bone graft substitute devices in bone regeneration. Mater Sci Eng C Mater Biol Appl 2021;130:112466.
[6] Szczęsny G, Kopec M, Politis DJ, Kowalewski ZL, Łazarski A, Szolc T. A review on biomaterials for orthopaedic surgery and traumatology: from past to present. Materials 2022;15(10).
[7] Wong SK, Wong YH, Chin KY, Ima-Nirwana S. A review on the enhancement of calcium phosphate cement with biological materials in bone defect healing. Polymers 2021;13(18).
[8] Jeong J, Kim JH, Shim JH, Hwang NS, Heo CY. Bioactive calcium phosphate materials and applications in bone regeneration. Biomater Res 2019;23:4.
[9] Pylostomou A, Demir Ö, Loca D. Calcium phosphate bone cements as local drug delivery systems for bone cancer treatment. Biomater Adv 2023;148:213367.
[10] Zhang Y, Lin T, Meng H, Wang X, Peng H, Liu G, et al. 3D gel-printed porous magnesium scaffold coated with dibasic calcium phosphate dihydrate for bone repair in vivo. J Orthop Translat 2022;33:13–23.
[11] Cui X, Huang C, Chen Z, Zhang M, Liu C, Su K, et al. Hyaluronic acid facilitates bone repair effects of calcium phosphate cement by accelerating osteogenic expression. Bioact Mater 2021;6(11):3801–11.
[12] Haque MA, Chen B. Research progresses on magnesium phosphate cement: a review. Construct Build Mater 2019;211:885–98.
[13] Fang B, Hu Z, Shi T, Liu Y, Wang X, Yang D, et al. Research progress on the properties and applications of magnesium phosphate cement. Ceram Int 2023;49(3):4001–16.
[14] Gu X, Li Y, Qi C, Cai K. Biodegradable magnesium phosphates in biomedical applications. J Mater Chem B 2022;10(13):2097–112.
[15] Gong C, Fang S, Xia K, Chen J, Guo L, Guo W. Enhancing the mechanical properties and cytocompatibility of magnesium potassium phosphate cement by incorporating oxygen-carboxymethyl chitosan. Regen Biomater 2021;8(1):rbaa048.
[16] Yu L, Gao T, Li W, Yang J, Liu Y, Zhao Y, et al. Carboxymethyl chitosan-alginate enhances bone repair effects of magnesium phosphate bone cement by activating the FAK-Wnt pathway. Bioact Mater 2023;20:598–609.
[17] Sarian MN, Iqbal N, Sotoudehbagha P, Razavi M, Ahmed QU, Sukotjo C, et al. Potential bioactive coating system for high-performance absorbable magnesium bone implants. Bioact Mater 2022;12:42–63.
[18] Liu W, Zhai D, Huan Z, Wu C, Chang J. Novel tricalcium silicate/magnesium phosphate composite bone cement having high compressive strength, in vitro bioactivity and cytocompatibility. Acta Biomater 2015;21:217–27.
[19] Shi Y, Yu L, Gong C, Li W, Zhao Y, Guo W. A bioactive magnesium phosphate cement incorporating chondroitin sulfate for bone regeneration. Biomedical Materials 2021;16(3).
[20] Kaiser F, Schroter L, Stein S, Kruger B, Weichhold J, Stahlhut P, et al. Accelerated bone regeneration through rational design of magnesium phosphate cements. Acta Biomater 2022;145:358–71.
[21] Ostrowski N, Roy A, Kumta PN. Magnesium phosphate cement systems for hard tissue applications: a review. ACS Biomater Sci Eng 2016;2(7):1067–83.
[22] Nabiyouni M, Brückner T, Zhou H, Gbureck U, Bhaduri SB. Magnesium-based bioceramics in orthopedic applications. Acta Biomater 2018;66:23–43.
[23] Zhang W, Wang N, Yang M, Sun T, Zhang J, Zhao Y, et al. Periosteum and development of the tissue-engineered periosteum for guided bone regeneration. J Orthop Translat 2022;33:41–54.
[24] Marupanthorn K, Tantrawatpan C, Kheolamai P, Tantikanlayaporn D, Manochantr S. Bone morphogenetic protein-2 enhances the osteogenic differentiation capacity of mesenchymal stromal cells derived from human bone marrow and umbilical cord. Int J Mol Med 2017;39(3):654–62.
[25] Dadsetan M, Guda T, Runge MB, Mijares D, LeGeros RZ, LeGeros JP, et al. Effect of calcium phosphate coating and rhBMP-2 on bone regeneration in rabbit calvaria using poly(propylene fumarate) scaffolds. Acta Biomater 2015;18:9–20.
[26] Han S, Paeng KW, Park S, Jung UW, Cha JK, Hong J. Programmed BMP-2 release from biphasic calcium phosphates for optimal bone regeneration. Biomaterials 2021;272:120785.
[27] Peng H, Yanbin Z, Bin W, Yang W, Yangyang L, Mei L, et al. An injectable and absorbable magnesium phosphate bone cement designed for osteoporotic fractures. Mater Today Chem 2024;38:102086.
[28] Arkin VH, Narendrakumar U, Madhyastha H, Manjubala I. Characterization and in vitro evaluations of injectable calcium phosphate cement doped with magnesium and strontium. ACS Omega 2021;6(4):2477–86.
[29] Zhao Y, Yu S, Wu X, Dai H, Liu W, Tu R, et al. Construction of macroporous magnesium phosphate-based bone cement with sustained drug release. Mater Des 2021:200.
[30] Roseti L, Parisi V, Petretta M, Cavallo C, Desando G, Bartolotti I, et al. Scaffolds for bone tissue engineering: state of the art and new perspectives. Mater Sci Eng C 2017;78:1246–62.
[31] Lv S, Qu T, Al-Ward H, Mu L, Qiu H, Zhang Y. Influence of monocalcium phosphate on the properties of bioactive magnesium phosphate bone cement for bone regeneration. Materials 2022;15(6).
[32] Cui J, Yi Y, Zhang J, Chai L, Jin H. Preparation and mechanical properties analysis of porous structure for bone tissue engineering. Bio Med Mater Eng 2022;33(6):465–76.
[33] Kanter B, Geffers M, Ignatius A, Gbureck U. Control of in vivo mineral bone cement degradation. Acta Biomater 2014;10(7):3279–87.
[34] Zhang J, Liu W, Schnitzler V, Tancret F, Bouler JM. Calcium phosphate cements for bone substitution: chemistry, handling and mechanical properties. Acta Biomater 2014;10(3):1035–49.
[35] Demir-Oguz O, Boccaccini AR, Loca D. Injectable bone cements: what benefits the combination of calcium phosphates and bioactive glasses could bring? Bioact Mater 2023;19:217–36.
[36] Liu D, Cui C, Chen W, Shi J, Li B, Chen S. Biodegradable cements for bone regeneration. J Funct Biomater 2023;14(3).
[37] Zhang D, Peng F, Tan J, Zhang Y, Wang F, Xie J, et al. Self-assembled ferric oxyhydroxide nanosheet on PEO-coated magnesium alloy with photocatalytic/photothermal antibacterial and enhanced osteogenesis activities. Chem Eng J 2022;437.

[38] Ahmed MM, Ameen MSM, Abazari M, Badeleh SM, Rostamizadeh K, Mohammed SS. Chitosan-decorated and tripolyphosphate-crosslinked pH-sensitive niosomal nanogels for Controlled release of fluoropyrimidine 5-fluorouracil. Biomed Pharmacother 2023;164:114943.
[39] Wickström SA, Niessen CM. Cell adhesion and mechanics as drivers of tissue organization and differentiation: local cues for large scale organization. Curr Opin Cell Biol 2018;54:89–97.
[40] Khalili AA, Ahmad MR. A review of cell adhesion studies for biomedical and biological applications. Int J Mol Sci 2015;16(8):18149–84.
[41] Adhikari U, Rijal NP, Khanal S, Pai D, Sankar J, Bhattarai N. Magnesium incorporated chitosan based scaffolds for tissue engineering applications. Bioact Mater 2016;1(2):132–9.
[42] Wei X, Zhou W, Tang Z, Wu H, Liu Y, Dong H, et al. Magnesium surface-activated 3D printed porous PEEK scaffolds for in vivo osseointegration by promoting angiogenesis and osteogenesis. Bioact Mater 2023;20:16–28.
[43] Delgado-Calle J, Bellido T. The osteocyte as a signaling cell. Physiol Rev 2022;102 (1):379–410.
[44] Vimalraj S. Alkaline phosphatase: structure, expression and its function in bone mineralization. Gene 2020;754:144855.
[45] Rico-Llanos GA, Borrego-González S, Moncayo-Donoso M, Becerra J, Visser R. Collagen type I biomaterials as scaffolds for bone tissue engineering. Polymers 2021;13(4).
[46] Komori T. Functions of osteocalcin in bone, pancreas, testis, and muscle. Int J Mol Sci 2020;21(20).
[47] Salhotra A, Shah HN, Levi B, Longaker MT. Synthetic and Bone tissue engineering graft substitutes: what is the future? Nat Rev Mol Cell Biol 2020;21:696–711. 2020/09/10 edn.
[48] Komori T. Regulation of bone development and extracellular matrix protein genes by RUNX2. Cell Tissue Res 2010;339(1):189–95.
[49] Tsuji K, Bandyopadhyay A, Harfe BD, Cox K, Kakar S, Gerstenfeld L, et al. BMP2 activity, although dispensable for bone formation, is required for the initiation of fracture healing. Nat Genet 2006;38(12):1424–9.
[50] de Klerk E, t Hoen PA. Alternative mRNA transcription, processing, and translation: insights from RNA sequencing. Trends Genet 2015;31(3):128–39.
[51] Sato T, Verma S, Andrade CDC, Omeara M, Campbell N, Wang JS, et al. A FAK/HDAC5 signaling axis controls osteocyte mechanotransduction. Nat Commun 2020;11(1):3282.
[52] Zhao Y, Bai L, Zhang Y, Yao R, Sun Y, Hang R, et al. Type I collagen decorated nanoporous network on titanium implant surface promotes osseointegration through mediating immunomodulation, angiogenesis, and osteogenesis. Biomaterials 2022;288:121684.
[53] Zhao SJ, Kong FQ, Jie J, Li Q, Liu H, Xu AD, et al. Macrophage MSR1 promotes BMSC osteogenic differentiation and M2-like polarization by activating PI3K/AKT/GSK3β/β-catenin pathway. Theranostics 2020;10(1):17–35.
[54] Shan Z, Xie X, Wu X, Zhuang S, Zhang C. Development of degradable magnesium-based metal implants and their function in promoting bone metabolism (A review). J Orthop Translat 2022;36:184–93.